Optical response of laser-doped silicon carbide for an uncooled midwave infrared detector

Geunsik Lim,[1] Tariq Manzur,[2] and Aravinda Kar[1,*]

[1]Laser-Advanced Materials Processing Laboratory, Department of Mechanical, Materials and Aerospace Engineering, College of Optics and Photonics, Center for Research and Education in Optics and Lasers (CREOL), University of Central Florida, Orlando, Florida 32816-2700, USA

[2]Science and Technology Lead, Imaging and Electronic Warfare, Undersea Warfare Electromagnetic Systems Development, Building 1319, 1176 Howell Street, Newport, Rhode Island 02841-1708, USA

*Corresponding author: akar@creol.ucf.edu

Received 7 September 2010; revised 12 January 2011; accepted 12 February 2011; posted 16 February 2011 (Doc. ID 134607); published 7 June 2011

An uncooled mid-wave infrared (MWIR) detector is developed by doping an n-type 4H-SiC with Ga using a laser doping technique. 4H-SiC is one of the polytypes of crystalline silicon carbide and a wide bandgap semiconductor. The dopant creates an energy level of 0.30 eV, which was confirmed by optical spectroscopy of the doped sample. This energy level corresponds to the MWIR wavelength of 4.21 μm. The detection mechanism is based on the photoexcitation of electrons by the photons of this wavelength absorbed in the semiconductor. This process modifies the electron density, which changes the refractive index, and, therefore, the reflectance of the semiconductor is also changed. The change in the reflectance, which is the optical response of the detector, can be measured remotely with a laser beam, such as a He–Ne laser. This capability of measuring the detector response remotely makes it a wireless detector. The variation of refractive index was calculated as a function of absorbed irradiance based on the reflectance data for the as-received and doped samples. A distinct change was observed for the refractive index of the doped sample, indicating that the detector is suitable for applications at the 4.21 μm wavelength.

OCIS codes: 040.0040, 040.3060, 040.5160, 280.0280.

1. Introduction

Although infrared (IR) focal-plane arrays (FPAs) have been widely used in many imaging systems, the demand for cameras and linear arrays sensitive to the mid-wave IR (MWIR) (3–5 μm) and long-wavelength IR (8–12 μm) is growing continually. These remote sensors are used in a variety of applications, including the detection and monitoring of chemicals in atmospheric and other environments, telecommunications, and semiconductor manufacturing systems [1–3]. These two wave bands exhibit excellent atmospheric transmission (>50%) compared to very low (<0.1%) transmission in the visible range. Also, the wave band 5–8 μm is not very good for atmospheric transmission, mostly due to water vapor in air. Most of the principal emission lines of gas molecules lie in the MWIR spectral range. Therefore, the MWIR band is suitable for detecting and monitoring pollution, relative humidity profiles, and the distribution of different gases, such as carbon monoxide and nitrous oxide, in the atmosphere [4,5].

IR detectors are made of narrow bandgap semiconductors because of the low energy (0.05–1.3 eV) of IR photons. Various materials are used for specific spectral ranges, which include indium gallium arsenide (InGaAs) for the 0.7–2.6 μm range, indium arsenide (InAs) for 1–3.8 μm, indium antimonide (InSb) for 1–6.7 μm, lead sulfide (PbS) for 1–3.2 μm, lead selenide (PbSe) for 1.5–5.2 μm, mercury-cadmium-telluride ($Hg_{1-x}Cd_xTe$) for 0.8–25 μm, and vanadium

0003-6935/11/172640-14$15.00/0

oxide (VO_x) for 2–16 μm. HgCdTe (MCT) is a variable-gap semiconductor depending on the composition of Hg and Cd, which is used as a crystalline intrinsic detector cell to produce IR detectors. The MCT detectors exhibit very high signal-to-noise ratio and very short response time [6–8]. To achieve this excellent performance, the MCT detectors require cryogenic cooling at 77 K, resulting in a costly and bulky detector system. The weak Hg—Te bond, which induces bulk, surface and interface instability, and the toxicity of Hg led to the development of detectors with other materials. Some of these detectors include Schottky barriers on silicon, SiGe heterojunctions, AlGaAs multiple quantum wells, GaInSb strain layer superlattices, high-temperature superconductors, and pyroelectric and silicon bolometers [6]. In spite of considerable efforts, operating these devices at room temperature has been very difficult, with the exception of thermal detectors.

Cooling is a major limitation of IR detectors and a number of devices has been investigated to overcome this problem. Photoconductors, photoelectromagnetic detectors, Dember effect detectors, and MCT photodiodes [9] were some of the devices studied for room temperature operation. Different types of uncooled thermal IR detectors, such as thermocouples and pyroelectric and ferroelectric detectors are currently available [10–12], and are based on different properties of materials. Microbolometer detectors are made of either vanadium oxide or amorphous silicon, while the ferroelectric detectors are made of barium strontium titanate. There are also bolometers that are optimized for broadband detection in the 3–5 and 8–14 μm wavelength regions simultaneously [13]. Much attention has been paid to uncooled IR detectors of other operating mechanism, such as the optomechanical IR imaging system with a bimaterial microcantilever array [14].

Recently, crystalline silicon carbide, which is a wide bandgap (3.0–3.23 eV) semiconductor with an excellent rad-hard property, high thermal conductivity (490 $W/m \cdot K$), and high melting temperature (3100 K peritectic temperature), has been used to fabricate a variety of radiation detectors. High-quality large-area x-ray detectors based on SiC Schottky diodes, and high-energy particle (alpha and beta particles) detectors have been demonstrated. The particle detectors are based on the interaction between the charges of the incident particles and the orbital electrons of the absorber atoms (e.g., SiC) [15–17]. The operation of conventional radiation detectors, which are generally based on Ge or Si as the absorber atoms, is limited by the radiation damage threshold and thermal stability of the absorber material.

In this paper, we have demonstrated an SiC-based uncooled optical detector for the MWIR range and the detector produces optical signals. The simplicity of this detector is that a doped SiC can be used directly as the photon detector without any further microelectronics device fabrication steps and any electrical connection to the doped sample. Also, the detector operates at room temperature. The wide bandgap of SiC offers a unique advantage for tuning its photon detectibility to a desired wavelength by doping it with an appropriate dopant. Ga has an acceptor energy level of 0.30 eV in 4H-SiC [18,19] corresponding to the 4.21 μm wavelength. The operating principle of the optical detector is that the electromagnetic (EM) waves of this wavelength excite electrons from the valence band to the dopant energy level. Consequently, the electron density changes in these two energy levels, which affects the refractive index of the semiconductor and, therefore, modifies the reflectance of the doped region. This change in the reflectance represents the optical response of the detector, which is probed with a He–Ne laser.

2. Fabrication of MWIR Optical Detector

An n-type 4H-SiC substrate was doped with Ga using a laser doping technique to fabricate a detector for the MWIR wavelength of 4.21 μm. The substrate was a small rectangular piece of length, width, and thickness 1, 1, and 0.0375 cm, respectively, which was cleaned by soaking in $H_2O_2 : H_2SO_4$ (1∶1 by volume) solution for 15 min. It was then rinsed with deionized water and dipped into buffered oxide etchant. The clean substrate was placed in a vacuum chamber that was pumped down to 1 mTorr vacuum. Bet *et al.* [20] discussed the details of the experimental setup. To dope the substrate, a metal–organic precursor, triethylgallium ($(C_2H_5)_3Ga$), was heated in a bubbler immersed in a water bath maintained at 100 °C and the precursor vapor was delivered to the vacuum chamber with carrier gas Ar. The substrate was simultaneously heated with a continuous wave Nd:YAG ($\lambda = 1064$ nm) laser to decompose the vapor at the laser-heated spot, which produces Ga atoms that subsequently diffuse into the substrate. This doping experiment was carried out under the following conditions: laser power =10.5 W, focal length of the laser-focusing lens =150 mm, laser beam diameter =200 μm, and the speed of the substrate =0.8 mm/s. The length and width of the doped region were both 0.3 cm in one quadrant at the top surface of the substrate. After the doping experiment, the sample was cleaned with a 45 wt. % KOH solution and then rinsed with acetone, methanol, and deionized water. This doped sample can be used directly as the MWIR detector without any further processing of the sample. Also, multiwavelength MWIR detectors can be fabricated on a single chip by doping its other three quadrants with other dopants.

A. Spectroscopic Analysis of the Dopant Energy Level

Two physical phenomena, laser heating of the substrate and diffusion of Ga atoms into the substrate, occur simultaneously during the above-mentioned laser doping process. To understand their effects, the optical properties of three types of samples, an as-received 4H-SiC substrate, a laser heat-treated sample prepared by heating an as-received substrate

under the same laser processing conditions as in the doping process, but without the Ga precursor inside the vacuum chamber, and a Ga-doped sample, were measured using a Bruker Vertex 70 Fourier transform infrared spectrometer equipped with a Helios IR microsampling accessory. The Helios combines a rapid scan speed of 100 spectra per second with an IR microscope of resolution 250 μm. The absorption spectra of the doped sample revealed a peak at 4.21 μm (0.30 eV) with 32% absorbance, which is higher than the 16% and 12% absorbances of the laser heat-treated and as-received samples, respectively, as shown in Fig. 1(a). The optical properties of the laser heat-treated sample indicate that laser heating does not modify the substrate significantly compared to the as-received sample. However, the doped sample exhibits additional absorption peaks at the wavelengths 4.63 μm (0.27 eV) and 4.95 μm (0.25 eV) in Fig. 1(a), which could be due to several reasons. Some of the Ga atoms might be at the interstitial sites of the silicon carbide lattice, which can modify the electronic structure and thereby affect the Ga acceptor energy level. Even when the Ga atoms are at the substitutional sites, they can occupy the Si or C lattice sites to form a p-type semiconductor with multiple acceptor levels. Also, the Ga atoms can cause mechanical stresses in the lattice due to their atomic size being different from the sizes of the Si and C atoms, which can affect the acceptor energy levels.

Out of these two additional peaks, the peak at 4.63 μm will also contribute to the detector response since a narrow bandpass filter of transmission range 4.08–4.81 μm is used in this study to extract the MWIR wavelengths from a broadband source of EM waves. The doped sample has a higher absorption coefficient than the as-received sample as listed in Table 1, indicating that the Ga dopant has increased the absorption characteristics of the substrate. These spectroscopic data, therefore, show that the Ga dopant atoms have modified the optical properties of the as-received sample.

The appearance of the additional absorption peaks could be due to the presence of impurities or other defects in the n-type 4H-SiC substrate, which might have been activated during the laser doping process. Using an SiC epilayer as the starting substrate can avoid the formation of such additional peaks because epilayers are much purer than the substrates obtained from bulk crystals. On the other hand, the detector response of this study can be considered to be due to two MWIR wavelengths, 4.21 and 4.63 μm, which indicates the possibility of fabricating tunable detectors.

3. Measurement of the Optical Response

The detector (doped region) was tested to examine the effect of the 4.21 μm wavelength on the optical response, i.e., the changes in the refractive index and reflectance, of the detector. It was placed above an IR source and a set of optical elements consisting

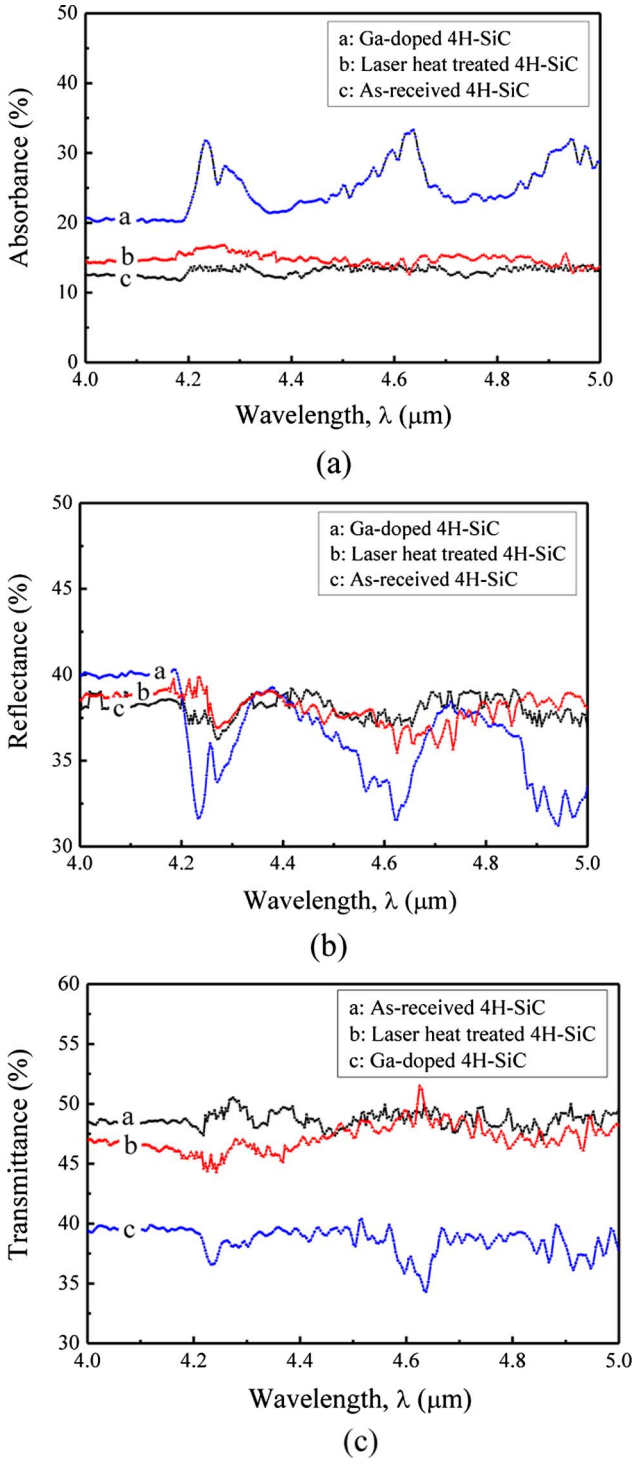

Fig. 1. (Color online) Spectroscopic data showing the optical properties of Ga-doped, laser heat-treated, and as-received 4H-SiC substrates: (a) absorbance, (b) reflectance, and (c) transmittance in the wavelength range 4–5 μm.

of two lenses and a filter, as shown in Fig. 2. The purpose of the optics is to focus the waves of 4.21 μm to the detector. A He–Ne laser of wavelength 632.8 nm was used to measure the changes in the reflectance. A stainless steel solid cylinder of diameter 25.4 mm and height 14.5 mm was heated to a very high temperature to form a heavily oxidized surface,

Table 1. Optical Properties of the As-Received and Doped 4H-SiC Substrates

Wavelength, λ	0.6328 μm		4.21 μm		4.63 μm	
Sample	As-received	Ga-doped	As-received	Ga-doped	As-received	Ga-doped
Absorbance	0.51	0.54	0.12	0.32	0.12	0.30
Reflectance	0.30	0.28	0.41	0.32	0.39	0.33
Transmittance	0.19	0.18	0.47	0.36	0.49	0.37
Reflectivity	0.26	0.25	0.29	0.19	0.27	0.20
Absorption coefficient (mm^{-1})	2.823	3.038	0.360	1.601	0.358	1.461
Absorption index	1.421×10^{-4}	1.530×10^{-4}	1.205×10^{-4}	5.362×10^{-4}	1.319×10^{-4}	5.384×10^{-4}
Refractive index	3.442	3.217	3.333	2.545	3.163	2.618

which was used as the MWIR radiation source. Siegel and Howell [21] reported that the emissivity of such a surface is 0.7 at 1200 K for the wavelengths 4.21 and 4.63 μm. At any wavelength λ and source temperature T, the spectral radiance of the stainless steel surface, $L_{\lambda,s}(\lambda, T)$, can be determined using the Planck blackbody radiation theory [22]. It is given by $L_{\lambda,s}(\lambda, T) = \varepsilon_{\lambda,s}(\lambda, T) \times L_{\lambda,b}(\lambda, T)$, where $\varepsilon_{\lambda,s}(\lambda, T)$ and $L_{\lambda,b}(\lambda, T)$ are the spectral emissivity of the stainless steel surface and the spectral radiance of blackbody, respectively. $L_{\lambda,s}(\lambda, T)$ is very small at room temperature for each of the wavelengths 4.21 and 4.63 μm. At 20 °C, the spectral radiances of the stainless steel surface are 0.541 and 0.969 $\mu W/mm^2 \cdot sr \cdot \mu m$ at 4.21 and 4.63 μm, respectively. At 25 °C, the spectral radiances are 0.658 and 1.158 $\mu W/mm^2 \cdot sr \cdot \mu m$ at 4.21 and 4.63 μm, respectively. So the detector needs to be very sensitive to detect any change in the source temperature, and the EM wave collection optics needs to be very high quality to collect the maximum amount of waves from the source and focus them to a small spot on the detector.

A. Optical Setup for Irradiance on the Ga-Doped SiC Sample

The stainless steel source emits EM waves over a broad band. from which a very small wavelength range around 4.21 μm was selected using a narrow bandpass filter. The filter had a high transmittance (~92.5%) in the range of 4.08–4.81 μm and a sharp cutoff outside this band. It is made of silicon monoxide and germanium thin films deposited on a silicon substrate and its safe operating temperature is below 200 °C. Therefore, it must be placed sufficiently away from the hot source to avoid any thermal damage to the filter.

To collect the EM waves from the source and direct them to the detector, two calcium fluoride (CaF_2) plano-convex lenses were used, as shown in Fig. 2. Because of high transmittance (~92%) in the range of 1–8 μm and high optical damage threshold (~10 J/cm^2 at the CO_2 laser wavelength of 10.64 μm), CaF_2 lenses are commonly used in cryogenically cooled thermal imaging systems. Its refractive index and melting temperature are 1.418 at 4.21 μm and 1418 °C, respectively. The diameter, center thickness, and effective focal length were 25.4, 6.2, and 50 mm for the source lens, and 25.4, 7.5, and 40 mm for the detector lens, respectively. The convex surfaces of both lenses were placed toward the incident waves (Fig. 2) to reduce the spherical aberration [23]. To determine the field of view, i.e., the area of the source from where the lens collects the EM waves, a ray tracing method was used [23,24]. Based on the dimensions of our experimental setup shown in Fig. 2, the diameters of the field of view and the irradiated spot on the detector are 25.4 and 3.8 mm, respectively.

If there is no energy loss when the radiation propagates from the source lens to the detector lens, the absorbed irradiance in the detector (I_a) can be written as

$$I_a(T) = \alpha_{d,\lambda} \frac{A_{rs}}{r_d^2} F_{\mathrm{sl}} \int_{\lambda_0 - \Delta\lambda_0/2}^{\lambda_0 + \Delta\lambda_0/2} L_{\lambda,s}(\lambda, T) \mathrm{d}\lambda, \qquad (1)$$

where $\alpha_{d,\lambda}$, A_{rs}, and r_d are the absorbance of the doped sample based on multiple reflections, the surface area of the radiation source as viewed by the source lens, and the radius of the irradiated spot on the detector for the MWIR wavelength λ, respectively. F_{sl} is the view factor as the source is viewed by the source lens, which is given by

$$F_{\mathrm{sl}} = \frac{1}{2}\left\{1 + \frac{d_{\mathrm{sl}}^2 + r_{\mathrm{sl}}^2}{r_{\mathrm{rs}}^2} - \left[\left(1 + \frac{d_{\mathrm{sl}}^2 + r_{\mathrm{sl}}^2}{r_{\mathrm{rs}}^2}\right)^2 - 4\left(\frac{r_{\mathrm{sl}}}{r_{\mathrm{rs}}}\right)^2\right]^{1/2}\right\}$$

for coaxial parallel disks [22], where r_{sl} and r_{rs} are the radii of the source lens and the radiation source, respectively, and d_{sl} is the distance from the radiation source to the source lens. λ_0 is the central wavelength to be detected by the detector and $\Delta\lambda_0$ is the spectral range, i.e., the full width at half-maximum around λ_0. From the absorbance data of Ga-doped 4H-SiC in Fig. 1(a), λ_0 would be 4.21 and 4.63 μm, corresponding to the two absorption peaks, and the values of $\Delta\lambda_0$ are 0.09 and 0.12 μm for these two wavelengths, respectively.

B. Measurement of Optical Signal for Testing the Response of the Ga-Doped Sample

The value of $I_a(T)$ needs to be maximized to optimize the change of the electron density in the valence and dopant energy levels of the detector. This will cause a large change in the reflectivity of the detector per unit change in the source temperature for the

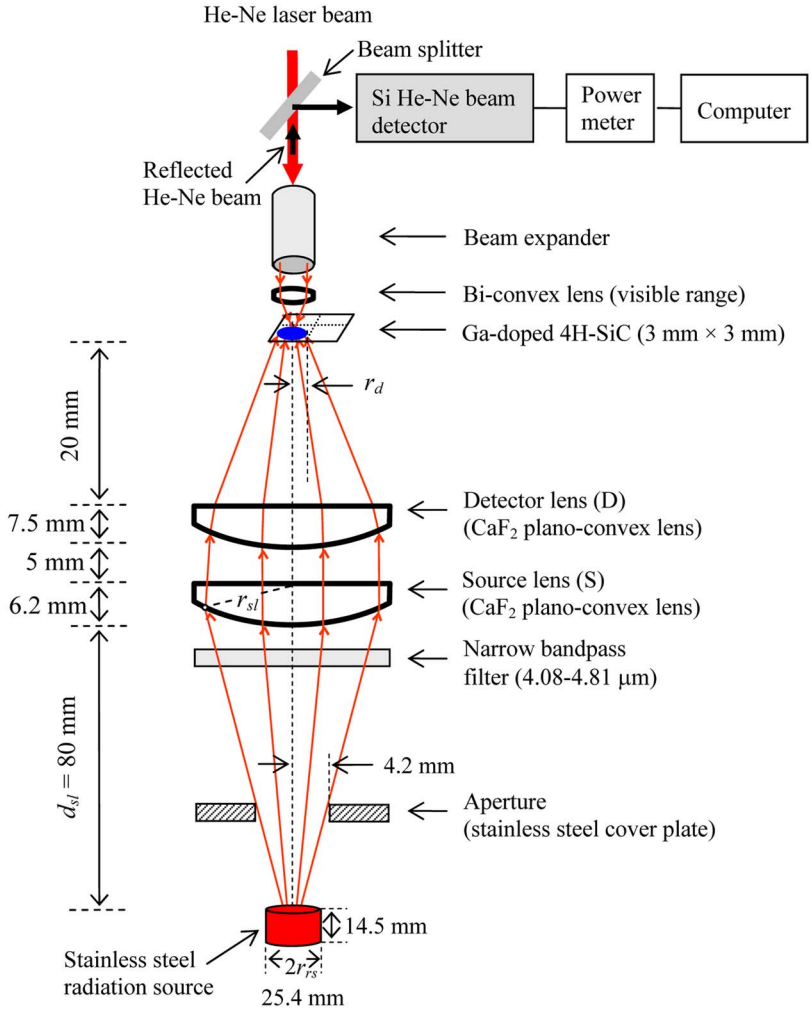

Fig. 2. (Color online) Optical arrangement to examine the detector response and ray geometry to calculate the irradiance on the SiC MWIR detector due to the radiance of a stainless steel source.

He–Ne laser of wavelength 632.8 nm, improving the detector response. The optical signal is the reflected power of the He–Ne beam, which is measured to test the effect of the source temperature on the detector response. The stainless steel source was heated using an induction heater and the surface temperature was measured with a thermocouple. The power input from the heater to the source was controlled to achieve stable source temperatures, which enabled carrying out detector response experiments at fixed temperatures.

To increase the irradiance at the detector surface, a ray tracing method was used for designing the MWIR radiation collection optics. The distances of the CaF_2 lenses were varied to obtain the largest source size (field of view) and the smallest irradiation spot on the detector (image size). The focal lengths of the source and detector lenses were 50 and 40 mm, respectively. The source and image radii were 12.7 and 1.9 mm, respectively, when the source lens, detector lens, and detector were at 80 mm from the source, 5 mm from the source lens, and 20 mm from the detector lens, respectively, as shown in Fig. 2. The narrow bandpass filter was placed right next to the convex surface of the source lens.

A He–Ne laser of wavelength 632.8 nm with an output power of up to 15 mW was directed to the detector (doped region) at normal incidence. The incident power of the He–Ne laser was measured right below the beam splitter in Fig. 2. The reflected laser beam was directed to a Si-based He–Ne detector, as shown in Fig. 2, to measure the reflected power that represents the optical signal of the SiC MWIR detector. The ratio of the reflected power to the incident power of the He–Ne beam yields the reflectance of the Ga-doped SiC sample. Experiments were conducted without any lens, with only the source lens, and with both the source and detector lenses to examine the effect of irradiance, $I_a(T)$, on the optical response of the SiC detector.

C. Multiple Reflections of the He–Ne Beam

Both the He–Ne laser beam and the MWIR waves can undergo multiple reflections in the 4H-SiC sample, increasing the absorption of photons in the detector. This will improve the quantum efficiency

and, therefore, the detector response. The undoped as-received sample offers two air–SiC interfaces at the top and bottom surfaces of the sample. On the other hand, the Ga-doped sample has three interfaces between the air and the doped region, the doped region and undoped silicon carbide, and undoped silicon carbide and air. When the He–Ne beam is incident on the top surface of the undoped as-received 4H-SiC region, a fraction of this beam is reflected, absorbed, and transmitted in the sample. These fragmented beams undergo further reflection and transmission at the bottom surface of the sample. Summing the powers of all the rays at various points on the top (reflectance) surface and on the bottom (transmittance) surface [25], the reflectances, ρ_{uj} and ρ_{dj}, and transmittances, τ_{uj} and τ_{dj}, of the undoped and doped samples are given by Eqs. (2) and (3), respectively, for the jth wavelength:

$$\rho_{u,j} = \rho_{au,j} + \frac{\rho_{au,j}(1-\rho_{au,j})^2 e^{-2\mu_{u,j}d_u}}{1-\rho_{au,j}^2 e^{-2\mu_{u,j}d_u}},$$
$$\tau_{u,j} = \frac{(1-\rho_{au,j})^2 e^{-\mu_{u,j}d_u}}{1-\rho_{au,j}^2 e^{-2\mu_{u,j}d_u}}, \tag{2}$$

and t_d is the diffusion time. Generally, t_d is taken as the laser–substrate interaction time, which is the ratio of the laser beam diameter on the substrate surface to the speed of the laser beam relative to the substrate. The value of t_d is 0.25 s for the doping experiment in this study. It has been shown that the diffusion coefficient increases by 5 to 6 orders of magnitude in laser doping processes and that the diffusion coefficient of aluminum (Al) atoms in silicon carbide is $1.2 \times 10^{-5}\,\mathrm{cm}^2/\mathrm{s}$ [26]. Assuming a similar trend for the diffusion of Ga, D_{Ga} was taken as $5.0 \times 10^{-5}\,\mathrm{cm}^2/\mathrm{s}$ to estimate d_d as 500 nm.

It should be noted that Eqs. (2) and (3) involve reflectivity and absorption coefficient. While the reflectivity depends only on material properties itself, reflectance depends on the material dimensions also [27]. The absorption coefficient (μ) is related to the absorption index (κ) by the expression $\mu = 4\pi\kappa/\lambda$, where λ is the wavelength of interest in vacuum. If the refractive and absorption indices of each of the two media are, respectively, n_1 and κ_1, and n_2 and κ_2, the Fresnel reflectivity at the interface of these two media is given by

$$\rho = \frac{(n_2-n_1)^2 + (\kappa_2-\kappa_1)^2}{(n_2+n_1)^2 + (\kappa_2+\kappa_1)^2}$$

$$\begin{aligned}
\rho_{d,j} &= \rho_{au,j} + \rho_{du,j}(1-\rho_{au,j})^2 e^{-2\mu_{u,j}d_u} + \frac{\rho_{du,j}^2 \rho_{au,j}(1-\rho_{au,j})^2 e^{-4\mu_{u,j}d_u}}{1-\rho_{du,j}\rho_{au,j}e^{-2\mu_{u,j}d_u}} + (1-\rho_{au,j})^2(1-\rho_{du,j})^2 \rho_{ad,j} e^{-2\mu_{u,j}d_u} e^{-2\mu_{d,j}d_d} \\
&\quad + \frac{(1-\rho_{au,j})^2(1-\rho_{du,j})^2 \rho_{au,j}\rho_{ad,j}\rho_{du,j} e^{-4\mu_{u,j}d_u} e^{-2\mu_{d,j}d_d}}{1-\rho_{au,j}\rho_{du,j}e^{-2\mu_{u,j}d_u}}, \\
\tau_{d,j} &= \frac{(1-\rho_{au,j})(1-\rho_{du,j})(1-\rho_{ad,j}) e^{-\mu_{u,j}d_u} e^{-\mu_{d,j}d_d}}{1-\rho_{ad,j}\rho_{du,j}e^{-2\mu_{d,j}d_d}} + (1-\rho_{au,j})(1-\rho_{du,j})^3(1-\rho_{ad,j})\rho_{au,j}\rho_{ad,j} e^{-3\mu_{u,j}d_u} e^{-3\mu_{d,j}d_d} \\
&\quad + \frac{(1-\rho_{au,j})(1-\rho_{du,j})^3(1-\rho_{ad,j})\rho_{au,j}\rho_{ad,j}\rho_{du,j} e^{-3\mu_{u,j}d_u} e^{-5\mu_{d,j}d_d}}{1-\rho_{ad,j}^2\rho_{du,j}e^{-2\mu_{d,j}d_d}},
\end{aligned} \tag{3}$$

where the subscripts $j = l$ and $j = \lambda$ represent the optical properties for the He–Ne laser and MWIR wavelengths, respectively. $\mu_{u,l}$ is the absorption coefficient of the undoped sample for the He–Ne laser wavelength and the thickness of the undoped as-received sample is $d_u = 0.375$ mm. The subscripts au, ad, and du represent the reflectivities at three interfaces, which are air–undoped SiC region, air–doped SiC region, and doped–undoped regions, respectively. $\mu_{d,j}$ and d_d are the absorption coefficient and thickness of the doped region, respectively.

The thickness of the doped region was taken to be the depth up to which the Ga atoms diffuse in the 4H-SiC substrate during the doping experiment. This diffusion length is given by $d_d = 2\sqrt{D_{\mathrm{Ga}} t_d}$, where D_{Ga} is the diffusion coefficient of Ga in the substrate for the wavelength λ. Utilizing these two expressions for absorption coefficient μ and reflectivity ρ in Eqs. (2) and (3), the refractive and absorption indices of the as-received and Ga-doped samples were calculated for the He–Ne laser and MWIR wavelengths for normal incidence on the samples at room temperature. These results are listed in Table 1. The reflectivity and absorption coefficient are two important parameters for determining the reflectance of the detector.

D. Analysis of the Reflected Power to Determine the Detectivity and the Noise-Equivalent Temperature Difference for the Ga-Doped Sample

Conventional photon detectors produce electrical signals. In such *electrical photodetectors*, the

photogenerated electrons migrate from the photon–detector interaction region to other parts of the detector and eventually flow through an electric circuit. An expression for the detectivity of this type of detectors can be found in [28]. On the other hand, the *optical photodetector* of this study produces optical signals. In this optical photodetector, the photoexcited electrons populate a higher energy level depending on their lifetime and diffusive loss in the excited state. The detectivities of these two types of detectors will, therefore, involve different parameters.

The functionality of the optical photodetector of this study involves two devices. One of them is the Ga-doped 4H-SiC substrate, which acts as the MWIR detector and produces optical signals by reflecting a He–Ne beam. The second device is the Si detector coupled with a powermeter, which detects the reflected He–Ne beam and measures its power. The detectivity, therefore, constitutes the performance of these two devices. The root mean square noise current is [29] $i_n = \sqrt{2e\bar{i}\Delta f}$ in the Si He–Ne beam detector, assuming that the shot noise in the detector is caused by the dc-photogenerated current $\bar{i}$ flowing across a potential barrier. Here e is the electron charge and Δf is the electrical bandwidth. The average output current, $\bar{i}$, is produced due to the incidence of background photons and the source photons on the SiC MWIR detector [29]. Since the photons are collected from the source using a lens and focused to a tiny spot on the detector, the irradiance on the detector would be much higher due to the source photons than the background photons.

In the presence of MWIR irradiance on the SiC detector, the average signal current, $\bar{i}_s$, can be expressed as $\bar{i}_s = \eta_{e,\mathrm{Si}} I^*_{r,l} \lambda_l A_{\mathrm{Si}} \alpha_{\mathrm{Si}} e/(hc)$, where $n_{e,\mathrm{Si}}$, A_{Si}, and α_{Si} are the external quantum efficiency, the active area, and the absorbance of the Si He–Ne beam detector, respectively. $I^*_{r,l}$ is the irradiance on the Si detector due to the reflected He–Ne laser in the presence of MWIR irradiance on the SiC detector and λ_l is the wavelength of the He–Ne laser. Therefore, $I^*_{r,l}\lambda_l/(hc)$ is the number of He–Ne laser photons incident on the Si detector per unit area per unit time. The irradiance can be related to the reflectance of the SiC MWIR detector by the expression $I^*_{r,l} = \rho^*_{d,l} I^*_{i,l}$, where $I^*_{i,l}$ is the irradiance of the He–Ne laser incident on the SiC detector and $\rho^*_{d,l}$ is the reflectance of the SiC detector for the He–Ne laser wavelength in the presence of MWIR irradiance.

In the absence of any MWIR irradiance on the SiC detector, the average noise current, $\bar{i}_n$, can be expressed as $\bar{i}_n = \eta_{e,\mathrm{Si}} I_{r,l} \lambda_l A_{\mathrm{Si}} \alpha_{\mathrm{Si}} e/(hc)$. Here $I_{r,l}$ is the irradiance on the Si He–Ne beam detector due to the reflected He–Ne laser in the absence of MWIR irradiance on the SiC MWIR detector. Identifying $\bar{i}_n$ as the average background current ($\bar{i}_{\mathrm{bg}}$), i.e., $\bar{i}_n = \bar{i}_{\mathrm{bg}} = \bar{i}$, and substituting it into the above-mentioned expression for i_n, the signal-to-noise ratio (S/N) can be written as $\bar{i}_s/i_n$, i.e.,

$$\frac{S}{N} = I^*_{r,l}\sqrt{\frac{\eta_{e,\mathrm{Si}} A_{\mathrm{Si}} \alpha_{\mathrm{Si}}}{2I_{r,l}\Delta f}}\sqrt{\frac{\lambda_l}{hc}}. \tag{4}$$

The minimum irradiance ($I^{*,m}_{r,l}$) for the detectable signal is obtained by setting $S/N = 1$ in Eq. (4), which yields $I^{*,m}_{r,l} = [2I_{r,l}\Delta f hc/(\eta_{e,\mathrm{Si}} A_{\mathrm{Si}} \alpha_{\mathrm{Si}} \lambda_l)]^{1/2}$. Therefore, the noise-equivalent power (NEP), which is given by $I^{*,m}_{r,l} A_{\mathrm{Si}}$, can be written as

$$\mathrm{NEP} = \sqrt{\frac{2I_{r,l} A_{\mathrm{Si}} \Delta f}{\eta_{e,\mathrm{Si}} \alpha_{\mathrm{Si}}}}\sqrt{\frac{hc}{\lambda_l}}. \tag{5}$$

The detectivity, which is defined as

$$D^* = \frac{\sqrt{A_{\mathrm{Si}}\Delta f}}{\mathrm{NEP}},$$

can now be written as

$$D^* = \sqrt{\frac{\eta_{e,\mathrm{Si}} \alpha_{\mathrm{Si}}}{2I_{r,l}}}\sqrt{\frac{\lambda_l}{hc}}.$$

This expression is modified using Eq. (4) and the expression for $I^*_{r,l}$ to obtain D^* as

$$D^* = \frac{S/N}{\rho^*_{d,l} I^*_{i,l}}\sqrt{\frac{\Delta f}{A_{\mathrm{Si}}}}. \tag{6}$$

Equation (6) combines the effects of both the Si He–Ne beam detector and the SiC MWIR detector. It can be used to determine the noise-equivalent temperature difference (NETD) based on the following equation [30]:

$$\mathrm{NETD} = \frac{4F^2}{D^* \tau_0 \left(\frac{dI_a}{dT}\right)_{\lambda_{1-}-\lambda_{2+}}}\sqrt{\frac{\Delta f}{A_d}}, \tag{7}$$

where F is the f-number of the detector lens, τ_0 is the product of the transmissivities of the lens and filter, and A_d is the active area of the detector. $(\frac{dI_a}{dT})_{\lambda_{1-}-\lambda_{2+}}$, which is the change in absorbed irradiance with respect to the source temperature in the emission band $\lambda_{1-} - \lambda_{2+}$, can be expressed as

$$\left(\frac{dI_a(T)}{dT}\right)_{\lambda_{1-}-\lambda_{2+}} = \left(\frac{\pi \varepsilon_{\lambda,s} A_{rs} F_{\mathrm{sl}} \alpha_{d,\lambda}}{A_d}\right) \times \left[\int_{\lambda_{1-}}^{\lambda_{1+}} \left\{\frac{C_1 C_2 \exp(C_2/\lambda T)}{T^2 \lambda^6 (\exp(C_2/\lambda T)-1)^2}\right\} d\lambda + \int_{\lambda_{2-}}^{\lambda_{2+}} \left\{\frac{C_1 C_2 \exp(C_2/\lambda T)}{T^2 \lambda^6 (\exp(C_2/\lambda T)-1)^2}\right\} d\lambda\right] \tag{8}$$

where C_1 and C_2 are two constants in Planck's blackbody radiation theory, which are given by $C_1 = 1.191 \times 10^8\,\mathrm{W}\cdot\mu\mathrm{m}^4/\mathrm{m}^2\cdot\mathrm{sr}$ and $C_2 = 1.439 \times 10^4\,\mu\mathrm{m}\cdot\mathrm{K}$. $\alpha_{d,\lambda}$ is the absorbance of the Ga-doped 4H-SiC sample, based on multiple reflections, for the MWIR wavelength λ, and the two emission bands are from $\lambda_{1-} = 4.2$ to $\lambda_{1+} = 4.29\,\mu\mathrm{m}$ and from $\lambda_{2-} = 4.54$ to $\lambda_{2+} = 4.66\,\mu\mathrm{m}$. $\varepsilon_{\lambda,s}$ is the emissivity of the stainless steel radiation source, which is 0.7 for these emission bands. Noting that $\alpha_{d,\lambda} = 0.32$, Eq. (8) yields $(\frac{dI_a}{dT})_{\lambda_{1-}-\lambda_{2+}} = 1.46 \times 10^{-3}\,\mu\mathrm{W/mm^2\cdot K}$. The transmissivities of the lens and filter are 1 and 0.925, respectively, at $4.21\,\mu\mathrm{m}$, yielding $\tau_0 = 0.925$. $F = 1/(2\sin\theta)$, where $\sin\theta$ is 12.5/21.65 in this case (Fig. 2) and, therefore, $F = 0.866$. The spectral photon radiance (photons/s $\cdot$ cm^2 $\cdot$ sr $\cdot$ μm) can be obtained by multiplying the absorbed irradiance by $\lambda/(hc)$. The detector absorbs a photon flux of 2.202×10^9 photons/s at 25 °C in the present setup. The reflected power of the He–Ne beam does not change if the absorbed photon flux is less than this value.

NETD was also determined from experimental data using the relationship [31] NETD $= \sigma_n/\mathrm{SITF}$, where σ_n and SITF are the standard deviation of the detector signal and the system intensity transfer function, respectively. Based on Bessel's correction to the conventional definition of the standard deviation, the expression for σ_n can be written as [32] $\sigma_n = \sqrt{[N\sum_{i=1}^{N} P_i^2 - (\sum_{i=1}^{N} P_i)^2]/(N(N-1))}$, where $P_i, i = 1, 2, 3, \cdots\cdots N$, is the ith value of the optical signal, i.e., the reflected power of the He–Ne beam, measured at different times to obtain N signals for the same source temperature. The SITF [31] of the detector is given by $\mathrm{SITF} = (\bar{P}_s - \bar{P}_{\mathrm{BG}})/(T_s - T_{\mathrm{BG}})$, where $\bar{P}_s$ and $\bar{P}_{\mathrm{BG}}$ are the averages of the N_s and N_{BG} values of the reflected He–Ne laser power for the source and background temperatures T_s and T_{BG}, respectively. Lloyd [30] pointed out how to select these two temperatures so that $T_s - T_{\mathrm{BG}}$ is not zero. Experiments were conducted to measure the variations in the reflected powers of the He–Ne beam by keeping the stainless steel radiation source at room (ambient) and higher temperatures. The data were recorded in a computer using a data acquisition system for a period of 25 s at each temperature as presented in Fig. 3. One-hundred values ($N = 100$) of the reflected He–Ne laser power were selected arbitrarily for each temperature to calculate NETD.

4. Results and Discussion

A. Changes in the Reflectance and Refractive Index of the SiC Detector as Functions of the Absorbed MWIR Irradiance

The SiC detector consists of two regions, which are the doped and undoped (as-received) regions. To calculate the optical properties of the detector, the properties of the doped region and the as-received sample were obtained. The reflected powers (P_r) of the He–Ne beam due to reflection by the SiC detector were measured using a silicon He–Ne beam detector by varying the temperature of the stainless steel radiation source from room temperature (25 °C) to 650 °C. For a given temperature of the source, its spectral radiance and its radiance within a finite spectral range are plotted as shown in Fig. 4(a). The source emits more radiation as its temperature increases and, consequently, the MWIR irradiance (W/cm^2) increases on the SiC detector. The reflectance is given by $\rho^*_{s,l} = P_r/P_i$, where $\rho^*_{s,l}$ represents the reflectance of the sample s, based on multiple reflections, for the He–Ne laser wavelength in the presence of MWIR irradiance on the sample. P_i is the power of the incident He–Ne beam on the sample, and $s = u$ and d for the undoped as-received and Ga-doped 4H-SiC samples, respectively. For each type of sample, the reflected power was also measured by keeping the stainless steel radiation source at room temperature, and the reflectance was calculated. This baseline reflectance is designated by $\rho_{s,b}$, which represents the reflectance of sample s for the He–Ne laser wavelength in the absence of any MWIR

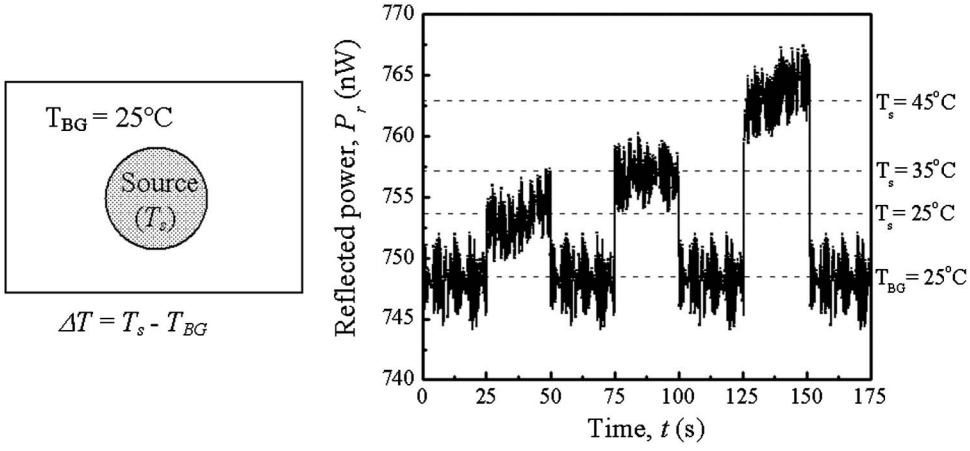

Fig. 3. Reflected powers of the He–Ne beam at room and higher temperatures of the source to determine NETD. T_{BG} is the background temperature of other materials surrounding the source. It is 25 °C in this study and the reflected power is lower than that of the source due to the difference in emissivity.

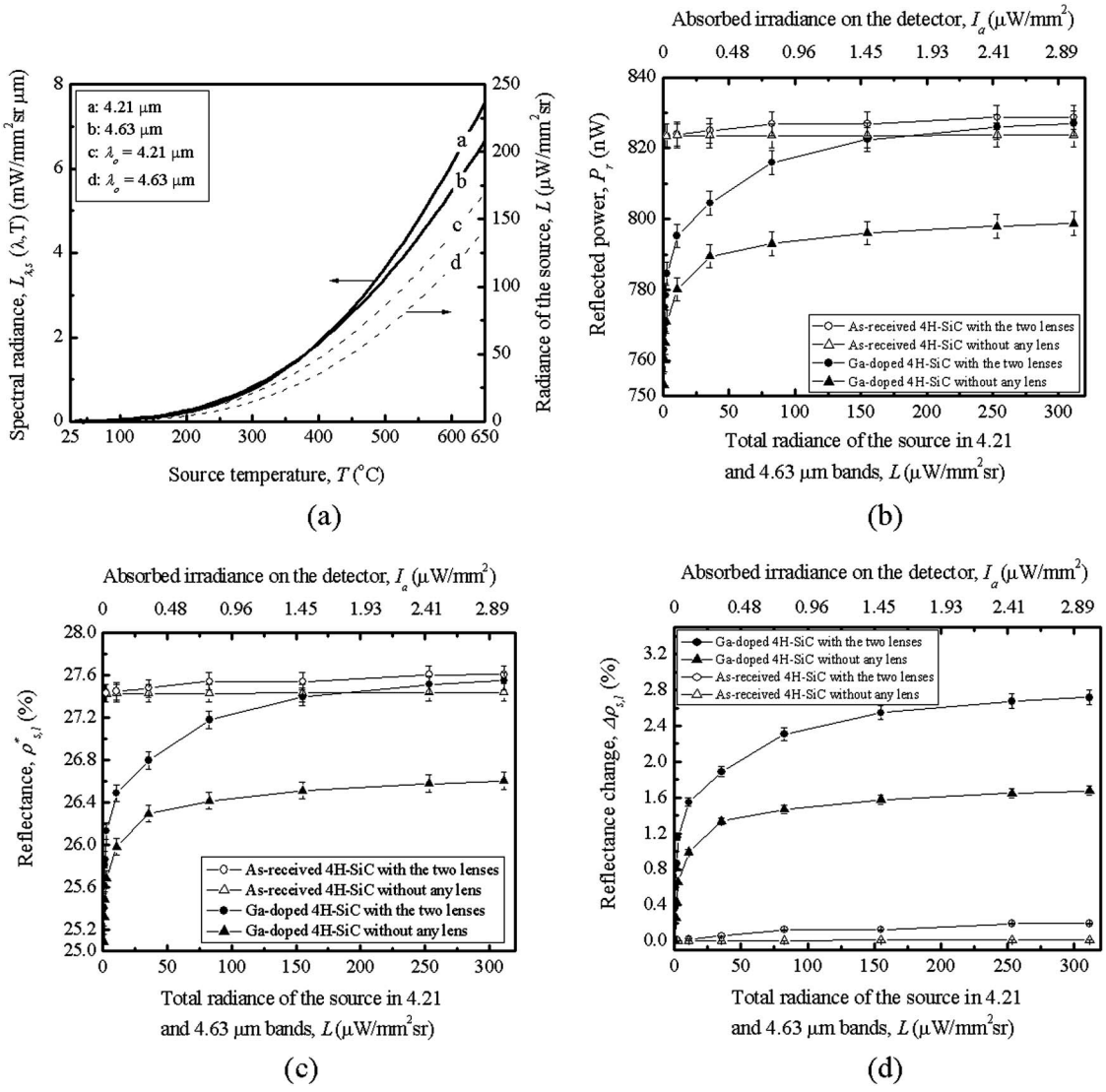

Fig. 4. Effects of the radiance of the source and the number of lenses on the optical response of the detector (Ga-doped sample) compared to the as-received (undoped) sample, showing that the doped sample produces a significant optical signal at the He–Ne laser wavelength of 632.8 nm: (a) effect of the source temperature on its radiance at two wavelengths, (b) reflected powers, (c) reflectances, and (d) changes in the reflectance of the as-received and Ga-doped samples. The resolution of the Si He–Ne beam detector was 0.63 nW.

irradiance on the sample from a hot source. The values of $\rho_{s,l}$ are found to be 26.47% and 25.02% for the undoped and doped samples, respectively. The change in the reflectance was obtained from $\Delta\rho_{s,l} = \rho_{s,l} - \rho^*_{s,l}$. These results are plotted in Figs. 4(b)–4(d), which show that the reflectance of the doped sample changes significantly due to the MWIR wavelengths 4.21 and 4.63 μm as the temperature of the radiation source increases, while the change is very small for the undoped as-received sample. More photon flux from the source at elevated temperatures and the presence of the Ga energy level corresponding to the photon energy in the doped sample are two important factors for better response of the doped sample than the undoped sample.

When the radiation source was at room temperature, the reflected and transmitted powers of the He–Ne beam were measured for both samples and the reflectance and transmittance were calculated. Using Eqs. (2) and (3), the baseline refractive ($n_{s,l}$) and absorption indices were calculated. $n_{s,l}$ represents the refractive index of sample s for the He–Ne laser wavelength in the absence of any MWIR irradiance on the sample from a hot source. The values of $n_{s,l}$ are found to be 3.442 and 3.217 for the undoped (as-received 4H-SiC) and Ga-doped samples, respectively. The absorption indices are found to be 1.421×10^{-4} and 1.530×10^{-4} for the undoped and doped samples, respectively, at the He–Ne laser wavelength of 632.8 nm. Based on these values of the $n_{s,l}$, absorption indices, and the reflectance data (Table 1) of the undoped and doped samples, the refractive index ($n^*_{s,l}$) of the SiC detector was calculated using Eqs. (2) and (3) for the He–Ne laser wavelength in the presence of MWIR irradiance on the sample. The

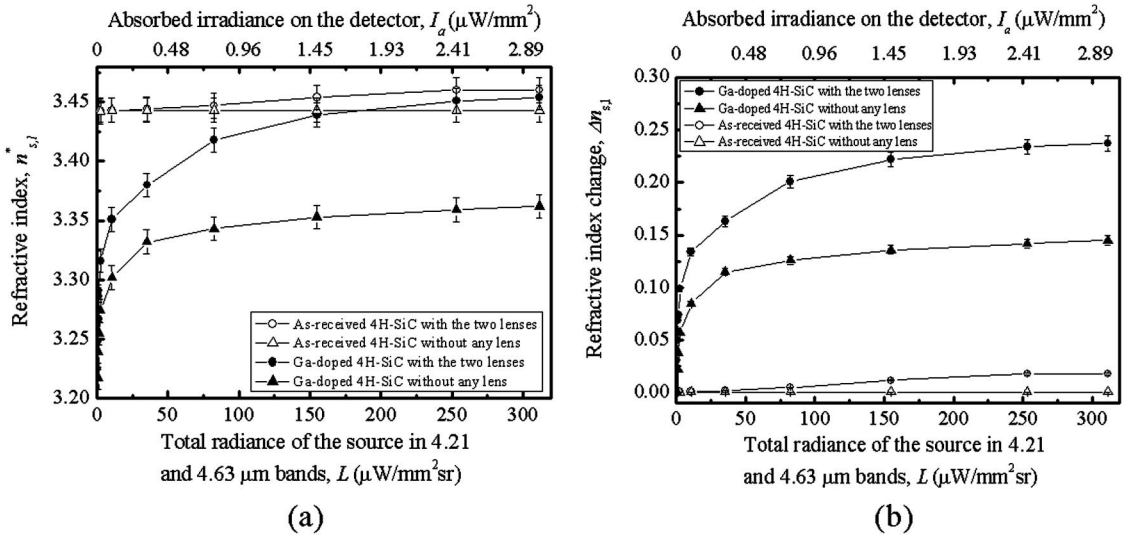

Fig. 5. Effects of the radiance of the source and the number of lenses on the refractive index of the detector compared to the as-received sample, showing a significant effect on the refractive index of the detector at the He–Ne laser wavelength of 632.8 nm: (a) refractive indices and (b) changes in the refractive index of the as-received and Ga-doped samples. The resolution of the Si He–Ne beam detector was 0.63 nW.

change in the refractive index was obtained from $\Delta n_{s,l} = n_{s,l} - n^*_{s,l}$. These results are plotted in Figs. 5(a) and 5(b), which show that the refractive index of the detector is distinctly different from the refractive index of the undoped sample in the presence of MWIR wavelengths 4.21 and 4.63 μm emitted by the radiation source. The doped sample has a lower refractive index in the presence of the MWIR irradiance because of the lower refractive index of the doped sample at room temperature than the undoped sample. Figure 5(b) shows a significant change in the refractive index of the doped sample, while the change is very small for the undoped sample. These significant changes in the reflectance and refractive index indicate that the Ga-doped sample can be used for fabricating MWIR detectors.

B. Effects of Radiation Collection Lenses and the Power Resolution of the Si He–Ne Beam Detector on the Low Signal Detectibility of the SiC Detector

To determine the minimum temperature of the radiation source for which the SiC detector produces a detectable optical signal, the radiation collection optics and the resolution of measuring the reflected He–Ne beam power by the Si detector were examined. Three optical arrangements were considered to collect the radiation, which are (i) no lenses, (ii) just one lens, and (iii) two lenses between the source and the SiC detector. The Si detector was operated in the nanowatt scale with the resolutions of 0.63 and 48 nW. At this low power level of the reflected He–Ne beam, the Si He–Ne beam detector exhibited an error of 0.3%. These results are presented in Figs. 6(a)–6(c). Figures 6(a) and 6(b) show the total radiance of the source in the 4.21 and 4.63 μm bands and absorbed irradiance on the SiC detector for a detectable response with no lenses, one lens, and two lenses as a function of the source temperature. A detectable response is obtained at a lower temperature (25 °C) with two lenses because two lenses collect more radiation from the source and produce higher irradiance on the SiC detector than the other two optical configurations. On the other hand, the He–Ne beam power measurement resolution of the Si detector also affects the radiation detection capability for a source of low temperature. It can be seen in Fig. 6(c) that the detector response begins at the source temperature 90 °C for 48 nW resolution, while a detectable signal is obtained for the source at room temperature with two lenses for 0.63 nW resolution. These results indicate that, although the SiC MWIR detector can operate at room temperature, the optics and the resolution of the Si detector are important in detecting objects that are at room temperature.

C. NETD and Detectivity

Experimental NETD. As pointed out in Subsection 3.D, the MWIR detection in this study involves the response of the SiC MWIR detector, and the responses of the Si He–Ne beam detector and the associated powermeter. The NETD of this SiC/Si detector system is calculated using the experimental values of the reflected He–Ne laser power (optical signal), as presented in Fig. 3. The average values of the signals are $\bar{P}_{r,1} = 753$ nW, $\bar{P}_{r,2} = 757$ nW, and $\bar{P}_{r,3} = 762$ nW at 25 °C, 35 °C, and 45 °C, respectively, and the corresponding standard deviations are $\sigma_1 = 9.342$ nW, $\sigma_2 = 6.257$ nW, and $\sigma_3 = 9.877$ nW. Applying SITF to two pairs of data at 25 °C and 35 °C, and at 25 °C and 45 °C, the SITFs are obtained as $\mathrm{SITF}_{12} = 0.5266$ nW/K and $\mathrm{SITF}_{13} = 0.7248$ nW/K, respectively, and the corresponding values of NETD are $\mathrm{NETD}_{12} = 1774$ mK and $\mathrm{NETD}_{13} = 863$ mK.

These values of NETD are much higher than the required thermal resolution of 100 mK. Thermal resolution below 100 mK is achieved in staring thermal imagers using thermal detectors in FPAs because NETD is influenced by the active area of the detector. For uncooled IR detector systems, Niklaus *et al.* [13] and Dong *et al.* [14] obtained an NETD of 7 K, while Picone [33] and Gupta and Ballato [34] reported NETD in the range of 50–100 mK. The SiC detector of this study can be configured as an FPA by laser doping selected regions of the substrate. To achieve low NETD, traditional IR detectors also typically have integrated circuit amplifiers or gain elements on the same microchip as the detector to amplify the signal by several orders of magnitude before being transmitted. These features are expected to lower the NETD of the uncooled SiC optical photodetector.

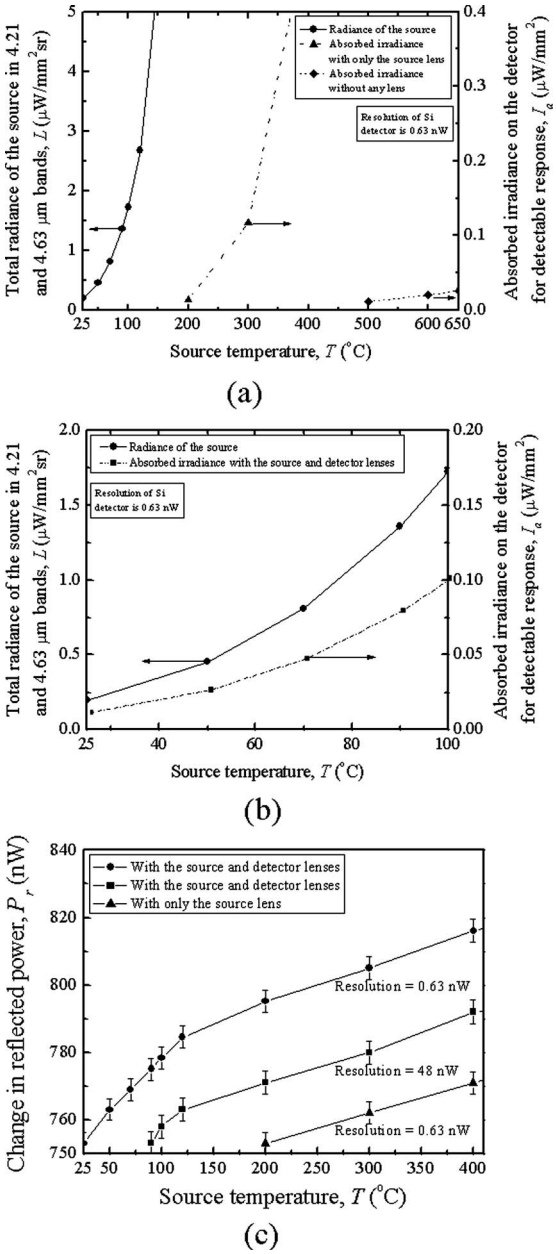

Fig. 6. Effects of the source temperature, the number of lenses, and the resolution of the Si He–Ne beam detector on the MWIR detectibility of the SiC detector: (a) threshold source temperature for MWIR detection with just the source lens and without any lens, (b) MWIR detection at room temperature (25 °C) with two lenses and 0.63 nW resolution of the Si detector, and (c) effects of the resolution of the Si detector on MWIR detection by the SiC detector, showing that two lenses and 0.63 nW resolution of the Si detector enable MWIR detection at room temperature of the source.

D^* based on experimental S/N. The detectivity of the SiC/Si detector system is determined from Eq. (6) using the experimental result for S/N and an appropriate value of Δf. Based on the data at room temperature (25 °C) in Fig. 3, $S/N = \bar{P}_{r,1}/\sigma_1 = 80.6$. The bandwidth is related to the time constant (t_c) of an instrument by the expression $\Delta f = 1/(2t_c)$. The results in Fig. 3 were obtained using a Si He–Ne beam detector coupled with a powermeter, for which the time constant is $t_c = 10$ ms. The time constant of the SiC MWIR detector is expected to be much lower than 10 ms. For example, different polytypes of SiC, such as 3C-, 4H-, and 6H-SiC, have fast (<20 ns) response times in photoconductive switches [35–39]. The response of a system, however, is governed by the component of longest time constant. Therefore, the bandwidth of the SiC/Si detector system is taken as $\Delta f = 50$ Hz. Other parameters for the results in Fig. 3 are the incident He–Ne laser irradiance on the SiC detector, $I^*_{i,l} = 26.786\,\mathrm{nW/mm^2}$, the reflectance of the SiC detector, $\rho^*_{d,l} = 0.28$ for the He–Ne laser wavelength, and the Si detector area $A_{\mathrm{Si}} = 1.131\,\mathrm{mm^2}$ for a He–Ne beam of diameter 1.2 mm. Substituting these values into Eq. (6), the detectivity of the SiC/Si detector system is found to be $7.15 \times 10^9\,\mathrm{cm \cdot Hz^{1/2}/W}$ when both the detector and the radiation source are at 25 °C.

The performances of various detectors at the 4.21 μm wavelength are listed in Table 2 to compare the characteristics of the SiC/Si detector system with other IR detectors. It should be noted that the optical configurations to collect IR radiation from the field of view might not be the same for all the detectors listed in Table 2, and that the radiation collection optics affects the NETD significantly. Also, the bandwidths are different for different detectors and that is why $D^*/\sqrt{\Delta f}$ is listed in Table 2, showing that this value of the SiC/Si detector system compares well with other detectors. However, the NETD of the SiC/Si detector system is very large, which can be reduced by increasing the S/N as discussed below.

Effect of Δf on D^*. Equation (6) shows that the detectivity can be increased by increasing the bandwidth of the detector. Newer models of Si He–Ne beam detectors with associated powermeters are available for which the time constant is $t_c = 2\,\mu$s with corresponding bandwidth $\Delta f = 2.5 \times 10^5$ Hz. With such fast Si detectors, the detectivity of the SiC/Si detector system would be $5.1 \times 10^{11}\,\mathrm{cm \cdot Hz^{1/2}/W}$. The detectivity of an ideal electrical photodetector [28] is $1.8 \times 10^{11}\,\mathrm{cm \cdot Hz^{1/2}/W}$ for the MWIR wavelength 4.21 μm when the radiation source is at 27 °C and the detector temperature is sufficiently low so

Table 2. Performances of Various Infrared Detectors at the 4.21 μm Wavelength

Detector	Operating Temp. (K) (Ref. [8])	Noise Bandwidth, Δf (Hz) (Ref. [8])	Detectivity, D^* (cm·Hz$^{1/2}$/W (Ref. [8])	NETD (mK)	$D^*/\sqrt{\Delta f}$
HgCdTe	77	1000	1.2×10^{11}	20 (Ref. [6])	3.8×10^9
InSb	77	1000	1.1×10^{11}	10 (Ref. [43])	3.5×10^9
PbSe	193	1000	3.3×10^{10}	200 (Ref. [33])	1.0×10^9
PtSi	300	30	3.0×10^{10}	100 (Ref. [44])	5.5×10^9
Au-doped Ge (Ge:Au)	77	1000	8.0×10^9	—	2.2×10^8
Thermocouple	300	10	1.8×10^9	100 (Ref. [33])	5.7×10^8
Pyroelectric	300	10	1.2×10^9	50 (Ref. [34])	3.8×10^8
Thermistor bolometer	300	10	1.9×10^8	50 (Ref. [13])	6.0×10^7
Thermopile	300	10	1.2×10^8	100 (Ref. [34])	3.8×10^7
SiC/Si detector system (this study)	298	50	7.15×10^9	1774	1.0×10^9

that the self-emission processes do not emit an appreciable number of photons. With lower time constants, the detectivity of the SiC/Si detector system would be higher than the ideal value because the SiC detector is based on the principle of generating optical signals with the photoexcited electrons remaining practically immobile inside the SiC detector. So the loss of photoexcited electrons occurs mainly due to their diffusion in this optical photodetector. In the conventional electrical photodetectors, on the other hand, electrical signals are produced due to photogenerated mobile electrons as they travel from the region of photon–detector interaction to other parts of the detector. So the loss of signal is due to both the scattering and diffusion of electrons in the electrical photodetectors.

Theoretical NETD. The detectivities and the corresponding values of Δf can be substituted into Eq. (7) to determine the theoretical NETD of the SiC/Si detector system. Noting that the active area of the SiC detector is $A_d = 1.131\,\text{mm}^2$ for a He–Ne beam of diameter 1.2 mm, and using the values of F, τ_0, and $(\frac{dI_a}{dT})_{\lambda_{1-}-\lambda_{2+}}$ that are discussed in Subsection 3.D, the theoretical values of NETD are found to be 207 and 205 mK for the SiC/Si detector systems of detectivities 7.15×10^9 and $5.1 \times 10^{11}\,\text{cm} \cdot \text{Hz}^{1/2}/\text{W}$, respectively. Ideally, these two values of NETD should be equal because it can be shown that NETD is independent of D^* and Δf by substituting D^* from Eq. (6) into Eq. (7). NETD is inversely proportional to S/N. The difference between the two values of NETD can be attributed to the computational rounding error. However, the theoretical NETD is much lower that the experimental NETD. This discrepancy between the theory and experiment might be due to the effect of $(\frac{dI_a}{dT})_{\lambda_{1-}-\lambda_{2+}}$. All the photons of the absorbed irradiance, $I_a(T)$, might not contribute to the generation of optical signal and, consequently, the theoretical value of $(\frac{dI_a}{dT})_{\lambda_{1-}-\lambda_{2+}}$ obtained from Eq. (8) might be higher than the actual occurrence in the SiC detector.

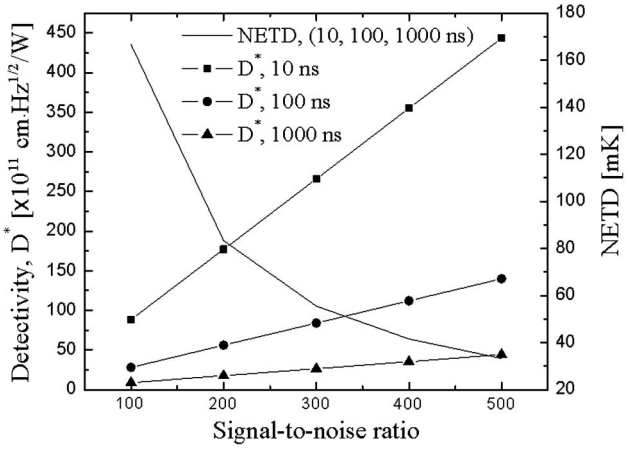

Fig. 7. Effects of S/N on the detectivity and NETD of just the SiC optical photodetector for three different time constants (10, 100, and 1000 ns) of the detector.

Effects of S/N and time constant on the detectivity and NETD of just the SiC detector. Bai *et al.* [40] fabricated 4H-SiC PIN avalanche photodiodes (APDs) for ultraviolet (UV, 280 nm wavelength) photon detection and demonstrated a fairly large detectivity of $4.1 \times 10^{14}\,\text{cm} \cdot \text{Hz}^{1/2}/\text{W}$. At the bias voltage of 144 V for this type of APD, Bai *et al.* [41] reported the NEP as 20 fW of incident light power and the highest incident light power as 4×10^3 fW, which leads to the S/N of ~200. They [41] were able to reduce the NEP to ~4.4 fW by using a lock-in amplifier, which significantly increases S/N to ~909. Qian *et al.* [42] fabricated a Si UV-sensitive photodetector and tested its response in the range of 300–650 nm at different bias voltages. Their detector consisted of separate photoabsorption and charge multiplication regions, which were a shallow p–n junction for photoelectric conversion and a nearby n–p–n output transistor for signal amplification, respectively. They were able to achieve S/N up to 7×10^6 with this particular amplification feature. The signal rise time of the photodetector was in the range of 2.16–750 ns for bias voltages varying from 1–20 V.

However, the operational mechanism of these electrical photodetector is different from the optical photodetector of this study. Equation (6) is used to determine the detectivity by replacing A_{Si} with A_d and referring all other variables, such as D^*, S/N, and Δf to the characteristics of just the SiC detector, while NETD is calculated using Eq. (7). To examine

the effects of S/N and Δf on D^* and NETD, S/N is varied from 100 to 500 for three different time constants, 10, 100, and 1000 ns, corresponding to $\Delta f = 5 \times 10^7$, 5×10^6, and 5×10^5 Hz, respectively. The results are presented in Fig. 7, showing that the detectivity is linearly proportional to S/N, while NETD is inversely proportional to S/N. Figure 7 also shows that the detectivity is affected by the time constant of the detector but the NETD is independent of the time constant for a given S/N. The NETD of the detector can be lowered by increasing its S/N.

5. Conclusion

We have fabricated an optical photodetector, which is an uncooled MWIR detector that produces an optical signal. The detector response can be measured remotely using a He–Ne laser beam. Ga atoms were incorporated into a 4H-SiC substrate by a laser doping technique to fabricate the MWIR detector because Ga creates an impurity energy level corresponding to the wavelength 4.21 μm. Optical spectroscopy of the doped sample reveals additional absorption peaks at the MWIR wavelengths of 4.63 and 4.95 μm. The presence of these peaks demonstrates the possibility of fabricating tunable detectors.

Significant changes in the reflectance and refractive index of the Ga-doped sample confirm that such samples can be used as MWIR detectors. The detector produced optical signals due to radiations from a stainless steel surface, which was at room temperature (25 °C), when two lenses were used as the MWIR radiation collection optics and the Si detector was operated at the subnanowatt resolution scale (0.63 nW) for measuring the change in the reflected He–Ne laser power. The detectivity of the SiC/Si detector system is 7.15×10^9 cm $\cdot$ Hz$^{1/2}$/W for the MWIR wavelength 4.21 μm. It can be increased to 5.1×10^{11} cm $\cdot$ Hz$^{1/2}$/W with a Si He–Ne laser detector of lower time constant, which is higher than the detectivity (1.8×10^{11} cm $\cdot$ Hz$^{1/2}$/W) of an ideal electrical photodetector. The increase in the detectivity might be because there is less loss of electrons in the optical photodetector than in the conventional electrical photodetectors. The NETD is found to be 1774 mK based on experimental data for the radiation source at 25 °C, while it is 207 mK based on theoretical calculation. Increasing the S/N and optimizing the radiation collection optics and dopant concentration will lower the NETD of the detector.

This work was supported by the Naval Undersea Warfare Electromagnetic Systems Development Program, Newport, Rhode Island, USA.

References

1. D. Scribner, J. Schuler, P. Warren, J. Howard, and M. Kruer, "Image preprocessing for the infrared," Proc. SPIE **4028**, 222–233 (2000).
2. M. Reine, "Review of HgCdTe photodiodes for IR detection," Proc. SPIE **4028**, 320–330 (2000).
3. M. Schlessinger, *Infrared Technology Fundamentals* (Marcel Dekker, 1995), pp. 77–92.
4. J. A. Jamieson, R. H. McFee, G. N. Plass, R. H. Grube, and R. G. Richards, *Infrared Physics and Engineering* (McGraw-Hill, 1963), pp. 43–73.
5. J. L. Miller, *Principles of Infrared Technology* (Van Nostrand Reinhold, 1994), pp. 106–176.
6. A. Rogalski, "HgCdTe infrared detector material: history, status and outlook," Rep. Prog. Phys. **68**, 2267–2336 (2005).
7. P. Norton, "HgCdTe infrared detectors," Opto-Electron. Rev. **10**, 159–174 (2002).
8. A. Rogalski, *Infrared Photon Detectors* (SPIE, 1995), pp. 1–11.
9. J. Piotrowski and A. Rogalski, "Uncooled long wavelength infrared photon detectors," Infrared Phys. Technol. **46**, 115–131 (2004).
10. S. J. Lee, Y. H. Lee, S. H. Suh, Y. J. Oh, T. Y. Kim, M. H. Oh, C. J. Kim, and B. K. Ju, "Uncooled thermopile infrared detector with chromium oxide absorption layer," Sens. Actuators A **95**, 24–28 (2001).
11. P. Muralt, "Micromachined infrared detectors based on pyroelectric thin films," Rep. Prog. Phys. **64**, 1339–1388 (2001).
12. M. Noda, K. Hashimoto, R. Kubo, H. Tanaka, T. Mukaigawa, H. Xu, and M. Okuyama, "A new type of dielectric bolometer mode of detector pixel using ferroelectric thin film capacitors for infrared image sensor," Sens. Actuators A **77**, 39–44 (1999).
13. F. Niklaus, C. Vieider, and H. Jakobsen, "MEMS-based uncooled infrared bolometer arrays—a review," Proc. SPIE **6836**, 68360D (2007).
14. F. Dong, Q. Zhang, D. Chen, L. Pan, Z. Guo, W. Wang, Z. Duan, and X. Wu, "An uncooled optically readable infrared imaging detector," Sens. Actuators A **133**, 236–242 (2007).
15. G. N. Violina, E. V. Kalinina, G. F. Kholujanov, V. G. Kossov, R. R. Yafaev, A. Hallen, and A. O. Konstantinov, "Silicon carbide detectors of high-energy particles," Semiconductors **36**, 710–713 (2002).
16. E. Vittone, N. Skukan, Z. Pastuovic, P. Olivero, and M. Jaksic, "Charge collection efficiency mapping of interdigitated 4H-SiC detectors," Nucl. Instrum. Methods Phys. Res. B **267**, 2197–2202 (2009).
17. F. Nava, G. Bertuccio, A. Cavallini, and E. Vittone, "Silicon carbide and its use as a radiation detector material," Meas. Sci. Technol. **19**, 102001 (2008).
18. A. A. Lebedev, "Silicon carbide: materials, processing, and devices," in *Deep-Level Defects in SiC Materials and Devices*, Z. C. Feng and J. H. Zhao, eds., Vol. 20 of Optoelectronic Properties of Semiconductors and Superlattices (Taylor & Francis, 2004), Chap. 4, pp. 121–163.
19. A. A. Lebedev, "Deep level centers in silicon carbide: a review," Semiconductors **33**, 107–130 (1999).
20. S. Bet, N. R. Quick, and A. Kar, "Laser doping of chromium as a double acceptor in silicon carbide with reduced crystalline damage and nearly all dopants in activated state," Acta Mater. **56**, 1857–1867 (2008).
21. R. Siegel and J. Howell, *Thermal Radiation Heat Transfer* (Taylor & Francis, 1994), pp. 60–131.
22. F. P. Incropera and D. P. DeWitt, *Introduction to Heat Transfer* (Wiley, 1985), pp. 611–613.
23. E. Hecht, *Optics* (Pearson Education, 2002), pp. 259–279.
24. J. E. Greivenkamp, *Field Guide to Geometrical Optics* (SPIE, 2004), pp. 7–30.
25. M. Rubin, "Solar optical properties of windows," Energy Res. **6**, 123–133 (1982).
26. Z. Tian, N. R. Quick, and A. Kar, "Laser-enhanced diffusion of nitrogen and aluminum dopants in silicon carbide," Acta Mater. **54**, 4273–4283 (2006).
27. C. A. Bennett, *Principles of Physical Optics* (Wiley, 2008), p. 87.
28. E. L. Dereniak and G. Boreman, *Infrared Detectors and Systems* (Wiley, 1996), p. 152–190.

29. E. L. Dereniak and D. G. Crowe, *Optical Radiation Detectors* (Wiley, 1984), p. 47.
30. J. M. Lloyd, *Thermal Imaging Systems* (Plenum, 1975), pp. 166–184.
31. Y. Li, D. Pan, C. Yang, and Y. Luo, "NETD test of high-sensitivity infrared camera," Proc. SPIE **6723**, 67233Q (2007).
32. W. H. Beyer, *Handbook of Mathematical Sciences* (CRC Press, Florida 1975), p. 727.
33. P. J. Picone, "Advanced infrared photodetectors (materials review)," Surveillance Research Laboratory Research Report, December 1993.
34. M. C. Gupta and J. Ballato, *The Handbook of Photonics* (CRC Press, 2006), pp. 6–32.
35. S. Sheng, M. G. Spencer, X. Tang, P. Zhou, K. Wongchotigul, C. Taylor, and G. L. Harris, "An investigation of 3C-SiC photoconductive power switching devices," Mater. Sci. Eng. B **46**, 147–151 (1997).
36. S. Dogan, A. Teke, D. Huang, H. Morkoc, C. B. Roberts, J. Parish, B. Ganguly, M. Smith, R. E. Myers, and S. E. Saddow, "4H-SiC photoconductive switching devices for use in high-power applications," Appl. Phys. Lett. **82**, 3107–3109 (2003).
37. F. Zhao, M. M. Islam, P. Muzykov, A. Bolotnikov, and T. S. Sudarshan, "Optically activated 4H-SiC p-i-n diodes for high-power applications," IEEE Electron Device Lett. **30**, 1182–1184 (2009).
38. P. S. Cho, J. Goldhar, C. H. Lee, S. E. Saddow, and P. Neudeck, "Photoconductive and photovoltaic response of high-dark-resistivity 6H-SiC devices," J. Appl. Phys. **77**, 1591–1599 (1995).
39. J. S. Sullivan and J. R. Stanly, "6H-SiC photoconductive switches triggered at below bandgap wavelengths," IEEE Trans. Dielectr. Electr. Insul. **14**, 980–985 (2007).
40. X. Bai, H.-D. Liu, D. C. McIntosh, and J. C. Campbell, "High-performance SiC avalanche photodiode for single ultraviolet photon detection," Proc. SPIE 7055, 70550Q (2008).
41. X. Bai, X. Guo, D. C. McIntosh, H.-D. Liu, and J. C. Campbell, "High detection sensitivity of ultraviolet 4H-SiC avalanche photodiodes," IEEE J. Quantum Electron. **43**, 1159–1162 (2007).
42. F. Qian, R. Schnupp, C. Q. Chen, R. Helbig, and H. Ryssel, "Indirect-coupling ultraviolet-sensitive photodetector with high electrical gain, fast response, and low noise," Sens. Actuators **86**, 66–72 (2000).
43. T. J. Phillips, "High performance thermal imaging technology," III-Vs Rev. **15**, 32–34 (2002).
44. A. Rogalski, "Infrared detectors: status and trends," Prog. Quantum Electron. **27**, 59–120 (2003).